bioRxiv preprint doi: https://doi.org/10.1101/2021.10.13.464316; this version posted October 15, 2021. The copyright holder for this preprint (which was not certified by peer review) is the author/funder, who has granted bioRxiv a license to display the preprint in perpetuity. It is made available under aCC-BY-NC-ND 4.0 International license.

CAR modulates plasma membrane nano-organization and immune signaling downstream of RALF1-FERONIA ligand-receptor signaling system

Weijun Chen[a, 1], Huina Zhou[b, 1], Fan Xu[a], Meng Yu[c], Alberto Coego[d], Lesia Rodriguez[d], Yuqing Lu[c], Qijun Xie[a], Qiong Fu[a], Jia Chen[a], Lan Li[a], Guoyun Xu[b], Dousheng Wu[a], Xiushan Li[a], Shaojun Dai[e], Xiaojuan Li[c], Yvon Jaillais[f], Pedro L. Rodriguez[d], Feng Yu[a, 2], Sirui Zhu[a, 2]

[a]State Key Laboratory of Chemo/Biosensing and Chemometrics, College of Biology, and State Key Laboratory of Hybrid Rice, Hunan University, Changsha 410082, P. R. China; [b]Zhengzhou Tobacco Research Institute, Zhengzhou 450001, P.R. China; [c]Beijing Advanced Innovation Center for Tree Breeding by Molecular Design, Beijing Forestry University, Beijing 100083, P. R. China; [d]Instituto de Biología Molecular y Celular de Plantas, Consejo Superior de Investigaciones Científicas–Universidad Politécnica de Valencia, ES–46022 Valencia, Spain; [e]Development Center of Plant Germplasm Resources, College of Life Sciences, Shanghai Normal University, Shanghai 200234, China; [f]Laboratoire Reproduction et Développement des Plantes, Université de Lyon, ENS de Lyon, CNRS, INRAE, F-69342 Lyon, France.

[1] W.-J.C. and H.-N.Z. contributed equally to this work.

[2] To whom correspondence may be addressed. Email: feng_yu@hnu.edu.cn (F.Y.); or sirui1115@hnu.edu.cn (S.R.Z.)

Abstract

The highly selective segregation of molecules at the plasma membrane (PM) to form domains is a widespread phenomenon. But how distinct signaling platforms are established and maintained by specific signals remains unclear. Here, we show that the receptor of Rapid Alkalinization Factor 1 (RALF1), the FERONIA (FER) receptor kinase, physically interacts with C2 domain ABA–related (CAR) proteins to control the nano-organization of the PM and to regulate extracellular signal transduction in *Arabidopsis*. During this process, the RALF1–FER pathway upregulates CAR protein

bioRxiv preprint doi: https://doi.org/10.1101/2021.10.13.464316; this version posted October 15, 2021. The copyright holder for this preprint (which was not certified by peer review) is the author/funder, who has granted bioRxiv a license to display the preprint in perpetuity. It is made available under aCC-BY-NC-ND 4.0 International license.

synthesis, which then controls the membrane lipid order. This might act as a rapid feedforward loop to stabilize FER in PM nanodomains. FER then interacts with and phosphorylates CARs, reducing their lipid-binding ability, which might break the feedback regulation and downregulate CAR activity at latter time point. Similar to *fer* mutant, a pentuple *car14569* mutant inhibits flg22-induced FLS2-BAK1 complex formation, which ultimately impacts plant immunity. Together, we proposed that the FER-CAR module controls the dynamics of the PM nano-organization during RALF signaling through a self-contained amplifying loop including both positive and negative feedbacks.

Introduction

Catharanthus roseus receptor–like kinase 1–like protein (*Cr*RLK1L) FERONIA (FER) is a receptor-like kinase with versatile and tissue–specific functions in plant cell growth and survival. FER functions with its ligands, rapid alkalinization factors (RALFs, e.g., RALF1 and RALF23), as a regulator of fertilization [1,2], cell growth [3-6], hormone signaling, stress responses [7], immune signaling [8] and energy and RNA metabolism [9-12]. However, the mechanism through which FER quickly responds to and integrates external signals and transmits them to varied downstream targets remains unknown. Recent report showed that FER acts as a scaffold to regulate the formation of the immune receptor complex (FLS2/BAK1) to respond to the bacterial pathogen–associated molecular pattern (PAMP) flagellin 22 (flg22) in a RALF–dependent manner [8]. In addition, structural data indicate that lorelei (LRE)–like2 (LLG2), a glycosylphosphatidylinositol (GPI)–anchored protein directly binds RALF23 to nucleate the assembly of RALF23–LLG2–FER heterocomplexes [13].

Biological membranes are made of a plethora of co-existing nanodomains, which are characterized by their small size (i.e., below 1 μm) [14-16]. Such membrane domains are critical in signaling notably because they can locally concentrate proteins, a process known as nanoclustering [16,17]. By increasing the local concentration of proteins, nanoclustering favors the formation of protein complexes or post-translational modifications, which often act as a trigger to initiate signaling. In addition, because

bioRxiv preprint doi: https://doi.org/10.1101/2021.10.13.464316; this version posted October 15, 2021. The copyright holder for this preprint (which was not certified by peer review) is the author/funder, who has granted bioRxiv a license to display the preprint in perpetuity. It is made available under aCC-BY-NC-ND 4.0 International license.

many different nanodomains coexist within the plane of the plasma membrane, they also ensure to formation of distinct complexes and thus signaling specificity [16]. Protein nanoclustering is regulated through the formation of various protein–lipid and protein–protein interactions [18-21]. As such, they act as versatile signaling platforms with very diverse composition in term of lipids and proteins [16,22,23]. Nanodomains also have several biophysical states, as they can be either in a liquid-disordered or a liquid-ordered phase [24]. GPI–anchored proteins such as LLG2 are inserted in the outer leaflet of the PM and they are often associated with sterol- and sphingolipid-rich liquid-ordered membrane domains [24,25]. A current hypothesis states that in plant cells, the RALF–FER module acts as a scaffold to provide a signaling platform to regulate immune receptor complexes [8]. Here, we hypothesized that RALF-FER may control the nanoclustering of diverse signaling complexes to achieve versatile and tissue–specific functions.

Accumulating evidence has shown that in plants, nanodomains are important for the cellular response to environmental cues and improving the fitness of plants [26-28]. For example, receptor–like kinases (RLKs), such as the brassinosteroid (BR) receptor BRASSINOSTEROID INSENSITIVE 1 (BRI1) [27] and the immune receptor FLAGELLIN SENSING 2 (FLS2), are located in distinct nanodomains to regulate either cell growth or immunity [29]. Furthermore, several works have linked the abscisic acid (ABA) response with nanodomain dynamics [26,30]. For example, a 10-member family of lipid–binding C2 domain ABA–related proteins (CARs, CAR1 to CAR10) was identified and found to interact with pyrabactin resistance 1 (PYR1)/PYR1-like (PYL)/regulatory components of ABA receptors (RCAR) ABA receptors and to positively regulate ABA signaling [31]. CARs oligomerize at the PM in a caclium-dependent manner [30,32]. However, the upstream regulator(s) that link CARs with the modulation of the PM landscape are still unknown. Herein, we propose a working model in which FER works together with lipid-binding CAR proteins to regulate the partitioning of signaling proteins into liquid-ordered/disordered membrane phases. In this scenario, RALF1 signaling elicits the formation of receptor complexes to quickly

bioRxiv preprint doi: https://doi.org/10.1101/2021.10.13.464316; this version posted October 15, 2021. The copyright holder for this preprint (which was not certified by peer review) is the author/funder, who has granted bioRxiv a license to display the preprint in perpetuity. It is made available under aCC-BY-NC-ND 4.0 International license.

respond to external signals by activating FER and regulating the accumulation and phosphorylation of downstream CAR proteins.

bioRxiv preprint doi: https://doi.org/10.1101/2021.10.13.464316; this version posted October 15, 2021. The copyright holder for this preprint (which was not certified by peer review) is the author/funder, who has granted bioRxiv a license to display the preprint in perpetuity. It is made available under aCC-BY-NC-ND 4.0 International license.

Results

The RALF1–FER pathway regulates Flot1 and FER localization in nanodomain and membrane order. Flot1 is a nanodomain–resident proteins from the reggie/flotillin family, that localizes in sterol-dependent liquid-ordered nanodomains in both animals [33] and plants [20,34]. Recently, Yu et al. (2020) reported that FER is located in nanodomains that colocalize with Flot1 [35]. To study whether RALF1–FER may impact Flot1 localization, we monitored GFP-Flot1 localization using variable–angle total internal reflection fluorescence microscopy (VA–TIRFM). When GFP–Flot1 was expressed in the *fer–4* background, both the density and size of GFP-Flot1 nanodomains significantly decreased (Fig. 1a-1c). By contrast, RALF1 treatment (1 µM, 10 min) increased the size of GFP-Flot1 nanodomains in a FER-dependent manner in the WT (Fig. 1a and 1b) but not in the *fer–4* background (Supplementary Fig. 1a- 1c). Next, we assessed the impact of RALF1–FER on Flot1 dynamics. First, we performed time-lapse analyses in VA-TIRFM followed by single particle tracking (SPT) to estimate the diffusion of GFP-Flot1-containing nanodomains. GFP-Flot1 nanodomains had a faster diffusion in the *fer–4* background than in the WT (Supplementary Fig. 1d). By contrast, they were more confined 10 min post RALF1 treatment (Supplementary Fig. 1e). Second, we addressed GFP-Flot1 dynamics using fluorescence recovery after photobleaching (FRAP) [36]. GFP-Flot1 had a faster and more complete fluorescence recovery in *fer-4* compared to the wild-type control (Supplementary Fig. 1f-1g). This confirmed that GFP-Flot1 diffuses more rapidly in the absence of FER. Consistent with our SPT analysis, RALF1 treatment led to a strong reduction in GFP-Flot1 fluorescence recovery, an effect that was entirely dependent upon the presence of FER (Supplementary Fig. 1f-1g). Together, our results suggest that RALF1–FER promotes Flot1 partitioning into nanodomains, likely by impacting Flot1 diffusion.

We noticed that the effect of *fer–4* on GFP–Flot1 localization in nanodomains resemble those induced by the sterol-depleting agent methyl–β–cyclodextrin (MβCD) (Fig. 1a, 1c and Supplementary Fig. 1d, 1e). This suggested that FER, like MβCD, may have a general effect on sterol-dependent membrane partitioning. To test whether

bioRxiv preprint doi: https://doi.org/10.1101/2021.10.13.464316; this version posted October 15, 2021. The copyright holder for this preprint (which was not certified by peer review) is the author/funder, who has granted bioRxiv a license to display the preprint in perpetuity. It is made available under aCC-BY-NC-ND 4.0 International license.

RALF1–FER directly impact membrane order, we took advantage of the lipid order–sensitive probe di–4–ANEPPDHQ [20,28,37]. When di–4–ANEPPDHQ molecules detect lipid domains with different dipole potentials in the cell membrane, there is a large shift in the peak emission wavelength of the dye from 630 nm in the liquid–disordered phase to 570 nm in the liquid–ordered phase (Supplementary Fig. 2a). The lipid-ordered phase will give a higher generalized polarization (GP) value (increased green fluorescence compared with red) [28]. To validate di–4–ANEPPDHQ in roots, we first used MβCD [28]. As expected, the GP value strongly decreased after MβCD treatment (Supplementary Fig. 2b). Similar to MβCD treatment, *fer–4* had significantly lower GP values than the WT, indicating a general decreased level of ordered lipid domains in the PM of this mutant (Fig. 1d and 1e). Furthermore, RALF1 promoted the formation of a liquid-ordered phase in WT in a FER-dependent manner (Fig. 1d and 1e). Taken together, our results suggest that RALF1–FER promotes the formation of liquid-ordered membrane domains, which is reflected by an increased localization of GFP-Flot1 in nanodomains.

Recently, a preprint paper by Gronnier et al. further showed that FER regulates the distribution of FLS2 and BAK1 in nanodomains in response to RALF23 [38]. Therefore, we hypothesize that FER nanoclustering is also regulated by RALF1, which may be important for FER to perform a variety of functions. Using VA-TIRF, we confirmed the presence of FER-GFP in nanodomains (Fig. 1f). Treatment with 1 μM RALF1 resulted in a significant increase in the size of FER–GFP particles (Fig. 1f and 1g), a decrease in the density of particles (Fig. 1h), which were more confined (i.e., lower diffusion coefficient, Supplementary Fig. 1e). To test whether this RALF1 effect on FER-GFP localization was dependent on sterol, we next treated *FER–GFP* plants with MβCD. This treatment dramatically hindered the formation of FER-GFP nanoclusters (i.e., lower density) (Fig. 1f and 1h) and the remaining FER-GFP-containing nanodomains had a faster diffusion than in the WT condition (Supplementary Fig. 1e). In addition, the effect of RALF1 on FER-GFP diffusion was fully suppressed by MβCD treatments (Fig. 1f, 1h and Supplementary Fig. 1e). Thus,

bioRxiv preprint doi: https://doi.org/10.1101/2021.10.13.464316; this version posted October 15, 2021. The copyright holder for this preprint (which was not certified by peer review) is the author/funder, who has granted bioRxiv a license to display the preprint in perpetuity. It is made available under aCC-BY-NC-ND 4.0 International license.

RALF1–FER has a general impact on membrane order, which regulate the very localization and dynamics of the FER module in a sterol-dependent manner.

Lipid-binding CAR proteins physically interact with the receptor kinase FER at the PM. To further understand the molecular mechanisms used by the RALF-FER pathway to modulate the compartmentalization of the PM, we performed a yeast two-hybrid (Y2H) screen using the cytoplasmic domain of FER (FER–CD, 469–896 amino acids, aa) as bait [5]. Among the interacting proteins, we found CAR9, which belongs to a 10-member family of lipid–binding C2 domain ABA–related proteins [30,31,39]. We cloned the full-length genes for the ten CAR family members (CAR1 – CAR10) and found that CAR1, CAR4, CAR5, CAR6, CAR9 and CAR10 were able to directly interact with FER–CD in Y2H assays (Fig. 2a and Supplementary Fig. 3a). Next, glutathione S–transferase (GST) pull–down assays further confirmed the interaction between CARs (GST-tagged CAR5, CAR6, CAR9 and CAR10) and His-tagged FER–CD (Fig. 2b). Furthermore, bimolecular fluorescence complementation (BiFC) assays were used to test the interaction between CARs and FER in *Arabidopsis* protoplasts. The results showed that CAR1, CAR4, CAR5, CAR6, CAR9, and CAR10 interacted with FER at the PM (the protein–protein interaction caused green fluorescence, which overlapped with FM4–64 PM red fluorescence) (Fig. 2c and Supplementary Fig. 3b). We next performed coimmunoprecipitation (co–IP) assays and confirmed the interaction between Myc–tagged CAR proteins (i.e., CAR4, CAR5, CAR6, CAR9, CAR10) and FER *in vivo* (Fig. 2d and Supplementary Fig. 3c). To further verify the specificity of the interaction between CAR and FER, we cloned the cytoplasmic domains of four *Cr*RLK1L family members (CVY1, AT2G39360; BUPS1, AT4G39110; MDS1, AT5G38990; MDS3, AT5G39020; HERK2, AT1G30570) and two LRR-RLKs (FLS2 and BRI1) and further analyzed their interaction with CAR9. The results of the Y2H assays showed that CAR9 interacted specifically with FER and BUPS1, but not the other six kinase domain, indicating that the interaction between FER and CAR9 is quite specific (Supplementary Fig. 3d). We also performed co–IP assays between Y2H noninteracting CARs (e.g., CAR3 and CAR7) and FER

bioRxiv preprint doi: https://doi.org/10.1101/2021.10.13.464316; this version posted October 15, 2021. The copyright holder for this preprint (which was not certified by peer review) is the author/funder, who has granted bioRxiv a license to display the preprint in perpetuity. It is made available under aCC-BY-NC-ND 4.0 International license.

(Supplementary Fig. 3e). The results revealed no major interaction of CAR3 and CAR7 with FER *in vivo*, which indicates that the interaction between certain CARs and FER is relatively specific. Taken together, these data suggest that FER physically interacts specifically with a subset of CAR proteins at the PM.

FER phosphorylates CARs, which further regulates the interaction of CAR with anionic lipids. To evaluate whether CARs could be substrates of FER, we first tested CAR5 and CAR9 by using *in vitro* phosphorylation assays (Fig. 3a). The results showed that FER–CD induced a significant phosphorylation–dependent shift in the CAR5 and CAR9 proteins (Fig. 3a). To further assess whether the phosphorylation levels of these two proteins were enhanced by the RALF1–FER signaling pathway *in vivo*, Phos–Tag–PAGE analysis [40] was used to detect pCAR5 and pCAR9 in plants expressing Myc-tagged CARs with or without RALF1 treatment (Fig. 3b). Notably, RALF1 treatment altered CAR protein abundance in *Arabidopsis* (detailed description below); thus, we adjusted the total protein levels (including those of phosphorylated and dephosphorylated proteins). We found a slow running form of CAR5 and CAR9, that was strongly reduced by alkaline phosphatase treatment (CIP), suggesting that they correspond to phosphorylated forms of CAR5 and CAR9 (thereafter referred to as pCAR5 and pCAR9). RALF1 treatment (1 μM, 30 minutes) increased the phosphorylation levels of both CAR5 and CAR9 *in vivo* (Fig. 3b). Time series analysis indicated that the phosphorylation level of CAR9-Myc increased at 20 min and 40 min post RALF1 treatment in the WT background but not in *fer-4* (Supplementary Fig. 4). A time series analysis of di–4–ANEPPDHQ staining revealed that lipid ordering increasing 5 minutes after RALF1 treatment and plateaued from 10 to 40 minutes of treatment with the peptide (Supplementary Fig. 5a-5b). Together, our results indicate that RALF1-mediated CAR9 phosphorylation is fully dependent on the presence of FER and is relatively slow compared to its effect on membrane order.

We further identified the FER-mediated phosphorylation sites of CAR5 and CAR9 using a previously developed ABA-induced coexpression system [6]. A kinase-dead

bioRxiv preprint doi: https://doi.org/10.1101/2021.10.13.464316; this version posted October 15, 2021. The copyright holder for this preprint (which was not certified by peer review) is the author/funder, who has granted bioRxiv a license to display the preprint in perpetuity. It is made available under aCC-BY-NC-ND 4.0 International license.

mutant of FER–CD (Lys at 565 was mutated into Arg, FER–CD^{K565R}) was used as a negative control [1]. Electrospray ionization (ESI) mass spectrometry (ESI-MS) analysis indicated that after ABA induction, FER phosphorylated CAR5 at Ser61, Ser62, and Tyr65 (Supplementary Fig. 6a–6c), and CAR9 at Thr26, Ser27, and Tyr30 (Supplementary Fig. 6d-6e), which are the equivalent phosphorylated residues in CAR5 (Supplementary Fig. 7). Interestingly, sequence alignment of CAR proteins (Supplementary Fig. 7) indicated that these three phosphorylation sites are located in the C2 domain [31]. Moreover, they are adjacent to the conserved Asp residues involved in Ca^{2+} binding [Asp22 and Asp27 in CAR1 and equivalent positions in other CARs [30]], which are highly conserved in CAR homologs from different species (Supplementary Fig. 7). Furthermore, 2 out of 3 sites were verified *in vivo* by label–free quantitative MS, and we found that RALF1 enhanced the CAR5 phosphorylation level at Ser62 and Tyr65 compared with mock-treated plants (Fig. 3c and Supplementary Fig. 6f). We further mutated the three amino acid residues of CAR5 and CAR9 to either alanine (Ala) or phenylalanine (Phe) (GST–CAR5^{3M}/9^{3M}, Ser and Thr were mutated into Ala, Tyr was mutated into Phe) [6,41] to test whether GST–CAR5^{3M} and GST–CAR9^{3M} were phosphorylated by FER–CD. As expected, GST–CAR5^{3M} and GST–CAR9^{3M} remained unphosphorylated by FER (Fig. 3d). These data suggest that RALF1 promotes the FER-mediated phosphorylation of CAR5 and CAR9 at specific sites within the Ca^{2+} and lipid binding pocket of their C2 domain.

The interactions between FER and its substrates were found to be regulated by their mutual phosphorylation [12]. We found that FER (+ ATP) (ATP activates FER self–phosphorylation) showed a higher affinity toward CAR9^{3M} than the kinase–dead FER–CD^{K565R} (+ ATP) form (Fig. 3e). In addition, CIP reduced the interaction of FER (+ ATP) but not FER–CD^{K565R} (+ ATP) with CAR9^{3M} (Fig. 3e). We then tested the effect of a CAR9 phosphorylation mimic on this interaction. We mutated three phosphorylation sites of CAR9 (Thr26, Ser27, Tyr30) to Asp (D) (GST–CAR9^{3D} mimics phosphorylated CAR9) to test how the negative charge introduced by these Asp residues affected the FER–CAR9 association. Compared with wild-type CAR9, GST–

bioRxiv preprint doi: https://doi.org/10.1101/2021.10.13.464316; this version posted October 15, 2021. The copyright holder for this preprint (which was not certified by peer review) is the author/funder, who has granted bioRxiv a license to display the preprint in perpetuity. It is made available under aCC-BY-NC-ND 4.0 International license.

CAR9^{3D} exhibited a lower association with FER–CD (41% ± 5.2% weakened) and FER^{K565R}–CD (42% ± 7.4% weakened) (Fig. 3f). These results indicated that the phosphorylation of FER promotes the FER–CAR9 interaction, whereas the phosphorylation of CAR9 reduces its affinity toward FER.

CAR has been identified to directly interact with anionic lipids *in vitro* [31]. To test whether FER regulates the interaction between CAR and anionic lipids via phosphorylation, we investigated the lipid–binding ability of CAR in phosphorylated and nonphosphorylated states [31]. First, we confirmed that many CAR proteins (CAR5, 6, 9, and 10) directly interact with anionic lipids [25:75 (w/w) mixture of phosphatidylserine:phosphatidylcholine] (Supplementary Fig. 8). Furthermore, we compared the effect of wild type FER and kinase-dead FER (FER^{K565R}) on CAR5 and CAR9 in lipid cosedimentation assays and found that phosphorylated CAR5 and CAR9 (coincubated with FER–CD and ATP) had a weakened capacity to interact with anionic lipids (Fig. 3g and 3h). Furthermore, comparison of the lipid binding ability of two mutant forms of CAR9 protein (GST–CAR9^{3M} and GST–CAR9^{3D}) toward liposomes revealed that CAR9^{3M} exhibited a similar association with liposomes than the wild-type CAR9, whereas CAR9^{3D} showed weaker binding ability toward anionic lipids (Fig. 3i). Taken together, FER phosphorylates CARs, which further regulates the FER–CAR interaction. Moreover, FER-mediated CAR phosphorylation reduces the lipid–binding ability of CARs.

The RALF1-FER-CAR axis promotes nanoclustering and lipid ordering in the PM. FER is located in nanoclusters and modulates the proportion of lipid ordering and the compartmentalization of the membrane, and CAR proteins interact with FER. Therefore, we hypothesize that RALF1-induced nanoclustering may further recruit CAR proteins into nanodomains, thereby affecting lipid ordering and membrane compartmentalization. Indeed, VA-TIRFM analysis showed that the YFP-CAR9 was located in nanoclusters under normal conditions (Fig. 4a). Treatment with 1 μM RALF1 increased YFP–CAR9 particle sizes and density in WT, while YFP-CAR9 clustering

bioRxiv preprint doi: https://doi.org/10.1101/2021.10.13.464316; this version posted October 15, 2021. The copyright holder for this preprint (which was not certified by peer review) is the author/funder, who has granted bioRxiv a license to display the preprint in perpetuity. It is made available under aCC-BY-NC-ND 4.0 International license.

decreased in the *fer-4* background (Fig. 4a-4c). Furthermore, similar to GFP-Flot1 and FER-GFP, diffusion analyses revealed that treatment with RALF1 induced a slower diffusion coefficient of YFP-CAR9 (Fig. 4d), and treatment with MβCD suggested that YFP-CAR9 nanoclustering was dependent on sterol (Fig. 4a and 4c). YFP-CAR9 nanodomains had a faster diffusion in the *fer–4* background than in the WT (Fig. 4d). Next, we assessed the impact of the phosphorylation level of CAR9 on its nanoclustering. We expressed the YFP-CAR9^{3D} and YFP-CAR9^{3M} in WT background, and VA-TIRFM analysis showed that YFP-CAR9^{3D} (dwell time 0.39 ± 0.16 s) and YFP-CAR9^{3M} (dwell time 0.88 ± 0.19 s) particles resulted in a shorter and longer dwell time than YFP-CAR9 (dwell time 0.64 ± 0.22 s), respectively (Fig. 4e and Supplementary Fig. 9).

To further confirm that CARs are required for the role of RALF1-FER in lipid ordering formation, a di–4–ANEPPDHQ stain assay was used to analyze lipid ordering in high–order CAR mutants, which were obtained by different combinations of single and multiple CAR mutants (see Methods for details). Compared to WT, the quadruple mutant *car1459* and the pentuple mutant *car14569*–Δ20 showed decreased liquid–ordered phase (Fig. 4f and 4g), indicating that lipid ordering in the PM is partly dependent on CAR proteins. Furthermore, *car14569*–Δ20 displayed substantial resistance to RALF1–induced lipid ordering compared to *car459* and *car1459* (Fig. 4f and 4g). We next analyzed lipid ordering in WT, *fer–4*, and CAR9–Myc/*fer–4* plants. When overexpressed in the *fer–4* background, CAR9–Myc partly rescued the lipid order defect of *fer–4* (Fig. 4h and 4i).

The RALF1-FER axis induced the formation of CAR9 nanoclusters with a larger size and increased density; thus, we asked whether RALF1–FER modulates the proportion of CAR in the nanodomain by promoting the accumulation of CAR proteins. A recent study showed that the RALF1–FER–eIF4E1 pathway partly promotes protein synthesis[12]. We then tested the protein accumulation of CARs using a pan–anti–CAR antibody (see Methods for details) (Supplementary Fig. 10a) and found that RALF1 triggered the rapid accumulation of CAR proteins, which was already detectable few

bioRxiv preprint doi: https://doi.org/10.1101/2021.10.13.464316; this version posted October 15, 2021. The copyright holder for this preprint (which was not certified by peer review) is the author/funder, who has granted bioRxiv a license to display the preprint in perpetuity. It is made available under aCC-BY-NC-ND 4.0 International license.

minutes post RALF treatment and picked 20 minutes after addition of the peptide (Supplementary Fig. 10b). Of note, the protein accumulation rate of CARs in the *fer–4* mutant was insensitive to RALF1 (Supplementary Fig. 10c). The RALF1–triggered rapid accumulation of CAR1, 4, 5, 6, 9, and 10 proteins was further confirmed in Myc–tagged transgenic plants (Supplementary Fig. 10d). Notably, the accumulation analysis of three CAR proteins (i.e., CAR2, CAR3 and CAR7), which have no direct interaction with FER, showed that RALF1 induced protein accumulation of CAR2 but not CAR3 or CAR7 (Supplementary Fig. 10e), suggesting that the RALF1 peptide and FER modulate CAR protein accumulation in a sophisticated manner, likely not dependent upon FER-CAR direct interaction. We thus tested whether the RALF1–FER complex modulated CAR mRNA translation using polysome profiling analysis [12], and found that RALF1 promoted the mRNA translation of *CAR1, 4, 5, 6, 9,* and *10* in WT (Supplementary Fig. 11a). Furthermore, the *fer–4* mutant blocked RALF1–triggered CAR1, 4, 5, 6, 9, and 10 mRNA translation (Supplementary Fig. 11b). These results demonstrate that RALF1–FER induces the rapid accumulation of CAR proteins likely prior to its recruitment to PM nanoclusters (Supplementary Fig. 11c).

The RALF1-FER-CAR axis participates in FLS2-BAK1 complex formation. Recently, a role of FER in the assembly of immune receptor complexes has been shown [8,13,38]. Our results suggest that CAR's ability to affect plasma membrane order might be central to stabilize FER signaling in response to RALF and to provide a platform for clustering of receptor complexes. To assess this hypothesis, we examined the flg22–induced association between FLS2 and its co–receptor BAK1 in *car14569*–Δ20 pentuple mutant. As previously described [8], the association of FLS2 and BAK1 was severely weakened in *fer-4* compared to WT after flg22 treatment (85% ± 4.5% reduction of the co–IP signal) (Fig. 5a and 5c). The co–IP of FLS2-BAK1 was also weakened in *car14569*–Δ20 after flg22 treatment compared to WT (25% ± 6.2% reduction), although less dramatically than in *fer–4* possibly because of residual CAR activity remaining in the pentuple *car* mutant (see discussion below) (Fig. 5b and 5c). Similar to RALF23 [8], the activation of FER by RALF1 inhibited FLS2 and BAK1

bioRxiv preprint doi: https://doi.org/10.1101/2021.10.13.464316; this version posted October 15, 2021. The copyright holder for this preprint (which was not certified by peer review) is the author/funder, who has granted bioRxiv a license to display the preprint in perpetuity. It is made available under aCC-BY-NC-ND 4.0 International license.

interaction induced by flg22 in the WT (48% ± 8.2% reduction) (Fig. 5a and 5c). In this co-signaling context, in the absence of FER (*fer-4*), RALF1 had no effect, whereas the residual CAR activity of the *car14569*–Δ20 mutant still mediated the RALF1 inhibitory effect on FLS2-BAK1 interaction, although less efficiently than in WT (compare WT lanes +flg22/+flg22+RALF1 with corresponding *car14569*–Δ20 lanes) (Fig. 5b and 5c). This suggests that a significant portion of RALF1's inhibitory effect on the flg22 induced association of FLS2–BAK1 is CAR dependent.

To examine the biological relevance of CARs' function in the RALF–FER pathway, we analyzed CAR's role in RALF1–FER–mediated immunity modulation. Flg22–induced ROS production was inhibited in pentuple CAR mutants (several *car14569* pentuple mutants were generated via CRISPR–Cas9 knockout of the *CAR6* gene in the *car1459* mutant background) (Fig. 5d and 5e), which, like *fer-4*, was more susceptible to the *Pseudomonas syringae pv.tomato* (*Pto*) DC3000, albeit not to the same extent (Fig. 5f). In addition, the pentuple CAR mutants were insensitive to the RALF1– and flg22–induced activation of mitogen–activated protein kinases (MAPKs) (Fig. 5g). These results demonstrate that the RALF1-FER-CAR axis plays a role in the formation of the FLS2-BAK1 complex and contributes to immunity response. Taken together, these findings indicate that CARs work together with the RALF1–FER pathway to regulate plant immune signaling.

bioRxiv preprint doi: https://doi.org/10.1101/2021.10.13.464316; this version posted October 15, 2021. The copyright holder for this preprint (which was not certified by peer review) is the author/funder, who has granted bioRxiv a license to display the preprint in perpetuity. It is made available under aCC-BY-NC-ND 4.0 International license.

Discussion

The molecular mechanisms through which eukaryotic cells modulate their PM landscape in response to external signals remain unclear [16]. Our study reveals that the FER-CAR module regulates the general lipid order of the membrane in response to an extracellular peptide, RALF1. MβCD treatment suggest that this effect is sterol-dependent, which is in line with the importance of some sterols in promoting the liquid-ordered phase of the membrane [24]. In turn, a number of proteins are stabilized in PM nanodomains, including the sterol-dependent Flot1 protein, but also FER and CAR themselves. CAR proteins directly interact with anionic lipids *in vitro*, including phosphatidylserine. Phosphatidylserine is present in membrane nanodomains in *Arabidopsis* root cells [23], which opens the possibility that CAR protein could be recruited to nanodomains via interaction with this lipid. CAR proteins interact with FER at the PM and are phosphorylated by the kinase (20 min after RALF1 treatment), thus weakening the ability of CARs to interact with anionic lipids. Such a mechanism might serve to fine tune the sensitivity of the system because upregulation of CAR proteins (within 10 min after RALF1 treatment) is also triggered by FER signaling.

An early and rapid response to the RALF1 peptide is the RALF1–FER–triggered Ca^{2+} wave [42]. Thus, it is reasonable to assume that the RALF1–FER–induced Ca^{2+} wave can further enhance the PM location of CAR proteins. In agreement with previous studies, we found that Ca^{2+} upregulates the lipid binding and membrane bending ability of CARs [30,31]. However, in the present study, we found that FER-dependent phosphorylation of CARs, which occurs in the proximity of conserved Asp residues involved in Ca^{2+} binding [30], seems to impair CAR binding to liposomes. Therefore, in the first minutes following RALF1 perception (<10 min), FER stimulates CAR proteins accumulation by upregulating its translation and might also trigger CAR membrane recruitment in a Ca^{2+}-dependent manner. In a second step (>20 min), the introduction of negative charges in the C2 domain of CARs by phosphorylation of specific Ser/Thr/Tyr residues might tune CAR binding to membranes. Mechanistically, the addition of negative charges within the lipid-binding pocket of CAR's C2 domain by

bioRxiv preprint doi: https://doi.org/10.1101/2021.10.13.464316; this version posted October 15, 2021. The copyright holder for this preprint (which was not certified by peer review) is the author/funder, who has granted bioRxiv a license to display the preprint in perpetuity. It is made available under aCC-BY-NC-ND 4.0 International license.

phosphorylation might repel the interaction with anionic phospholipid in the PM, such as phosphatidylserine or phosphatidylinositol-4-phosphate [43,44]. Thus, the system appears to be designed for a fast self-amplified recruitment of CAR in PM nanodomains, followed by a brake mechanism leading to CAR membrane dissociation. This scenario becomes even more complex when considering that RALF1–FER signaling is a master regulator of cell wall integrity [45], and the cell wall also has profound roles in the diffusion coefficients and PM compartmentalization of resident proteins [16,36,46-48].

Organization by compartmentalization can efficiently facilitate and orchestrate biological events in space and time [18]. Recently, Yu et al. showed that FER participates in the Flot1–dependent endocytosis pathway [35]. Herein, we found that FER and CAR are located in sterol-dependent nanodomains. It is possible that sterol–rich nanodomains provide compartmentalization for FER scaffolding function to modulate other receptor kinase complexes (e.g., FLS2 and BAK1), which then interact with their downstream effectors; therefore, FER could promote the integration of multiple environmental cues. Various studies indicate that FER regulates many aspects of plant biology, including growth, development, environmental adaptability, and immunity, by sensing a variety of external signals [45,49]. Similarly, we also found a pleiotropic phenotype in the high–order CAR mutants [31], indicating CAR-mediated regulation of membrane order could be pivotal for additional signaling systems.

Interesting future research topics include whether RALF1–FER regulates various cell type–specific outputs and/or signaling events via the dynamic nanoclustering of proteins and lipids (involving other receptor kinase complexes, ROPs, CARs and phosphatidylserine) of the PM. More studies are also needed to verify whether signal–triggered PM compartmentalization based on kinase receptors and C2 domain–containing proteins is a common mechanism in eukaryotic cells. In addition, previous evidence indicates that CAR proteins are located not only in the PM but also in the cytoplasm and nucleus, where these proteins participate in ABA signaling [31] and interact with LOT1 to enhance plant drought tolerance [39]. It would be interested to address whether the RALF1-mediated regulation of CAR accumulation, its recruitment

bioRxiv preprint doi: https://doi.org/10.1101/2021.10.13.464316; this version posted October 15, 2021. The copyright holder for this preprint (which was not certified by peer review) is the author/funder, who has granted bioRxiv a license to display the preprint in perpetuity. It is made available under aCC-BY-NC-ND 4.0 International license.

membrane interaction dynamics, and its phosphorylation may also impact ABA signaling.

bioRxiv preprint doi: https://doi.org/10.1101/2021.10.13.464316; this version posted October 15, 2021. The copyright holder for this preprint (which was not certified by peer review) is the author/funder, who has granted bioRxiv a license to display the preprint in perpetuity. It is made available under aCC-BY-NC-ND 4.0 International license.

Materials and Methods

Plant Material and Growth Conditions. *Arabidopsis thaliana* seeds were first surface sterilized by 75 % alcohol. After stigmatization at 4 °C for 3 d, seeds were growing on 1/2 MS with 0.8 % sucrose and 1.0 % Phytagel (Sigma–Aldrich) at 22 °C in a 16–h light/8–h dark condition for subsequent analysis. The *car5* (SAIL_802_B08), *car6* (SALK_052572.54.00.x), *car9* (SALK_088115.56.00.X), *car10* (SALK_122977C) T–DNA insertion mutants were obtained from the Salk Institute (http://signal.salk.edu). The double mutants *car56*, *car59* were respectively obtained by crossing *car5* (SAIL_802_B08) with *car6* (SALK_052572.54.00.x) and crossing *car5* (SAIL_802_B08) with *car9* (SALK_088115.56.00.X), then confirmed by PCR with specific primers (Supplemental Table 1). The *car145*, *car149*, *car459* and *car159* triple mutants were previously described[31]. The *car1459* mutant was generated in this work by crossing *car145* with *car149* and genotyping of the F2 seeds with primers described by Rodriguez et al., (2014)[31]. Next, several *car14569* pentuple mutants were generated in Dr. Pedro L. Rodriguez's laboratory via CRISPR–Cas9 knockout of the *CAR6* gene in the *car1459* mutant background. Several *car6* alleles were thus obtained. The *car6* allele (termed *car6*–Δ20) in *car14569*–Δ20 loses the sequence "GAAGGAACTGGTAGGGCTTG" (from 30–49 bp) respect to *CAR6*; the *car6* allele (termed *car6*–Δ10) in *car14569*–Δ10 loses the sequence "AACTGGTAGG" (from 36–47 bp), the *car6* allele (termed *car6*–Δ4) in *car14569*–Δ4 loses the sequence "AGGG" (43–46 bp) and the *car6* allele (termed *car6*–Δ1) in *car14569*–Δ*1* loses the nucleotide 43. A single guide RNA (sgRNA) targeting *CAR6* close to the N–terminus was designed using the online tool CRISPR–PLANT (http://www.genome.arizona.edu/crispr/CRISPRsearch.html). Thus, a 19-bp sequence (GAGGTTGAGATGAAGGAAC) followed by the TGG PAM sequence was selected and cloned as a guide-RNA into the entry vector pMTN2982 (GenBank accession number MG917725.1). The sgRNA driven by Arabidopsis U6–26 promoter was cloned into the pHEE2E-TRI vector (Addgene Plasmid #71288), which expresses Cas9 driven by the egg cell-specific EC1.2 promoter[27]. Transformed plants were selected in medium MS supplemented with 20 μg/mL hygromycin and a CAR6 fragment was amplified and

bioRxiv preprint doi: https://doi.org/10.1101/2021.10.13.464316; this version posted October 15, 2021. The copyright holder for this preprint (which was not certified by peer review) is the author/funder, who has granted bioRxiv a license to display the preprint in perpetuity. It is made available under aCC-BY-NC-ND 4.0 International license.

427 sequenced using the following primers: CAR6g-F
428 (AGTAGTAGAGTCAGGAGACAGG) and CAR6g-R
429 (GATTCTTTGGTCTTCCATCTGCG).

430 For overexpression assays, full–length coding sequences of *CAR4,5,6,9,10*
431 respectively fused with a C–terminal Myc tag driven by the ACT2 promoter were
432 cloned into pDT1[12]. We obtained transgenic plants *CAR1,4,5,6,9,10–Myc* in WT (Col–
433 0) background by *Agrobacterium*–mediated transformation. The transgenic plant
434 CAR9–Myc/*fer–4* was obtained by *Agrobacterium*–mediated transformation of CAR9–
435 Myc in *fer–4* background. The transgenic plant GFP–Flot1/*fer–4* was obtained by
436 crossing the *GFP–Flot1* plants with *fer–4* mutants. In the F2 generation, the *fer–4*
437 background was genotyped by PCR using gene–specific primers (Table S1). Wild–type
438 (Col–0), *fer–4* [4], *llg1–2* [2], *35S::YFP–CAR9* [39] and *GFP–Flot1*[34] were previously
439 described.

440 **Yeast Two–Hybrid (Y2H) Assay.** Y2H assays were performed as previously
441 described[50]. Briefly, the cytoplasm domain of *Cr*RLK1L family members (AT3G51550,
442 FER, 469–896 amino acids; AT2G39360, CVY1, 429–815 amino acids; AT5G38990,
443 MDS1, 462–880 amino acids; AT5G39020, MDS3, 459–813 amino acids; AT1G30570,
444 HERK2, 451–849 amino acids), and two RLKs (AT5G46330, FLS2, 870–1155 amino
445 acids; AT4G39400, BRI1, 814–1196 amino acids) were fused in–frame with the GAL4
446 DNA–binding domain of the bait vector pGBKT7. The CDS of of *CARs* were fused
447 with the GAL4 DNA–activating domain of the prey vector pGADT7 (AD–CAR).
448 Distinct plasmid pairs were transformed into yeast AH109 cells. The diluted
449 transformants were plated onto synthetic dropout medium lacking tryptophan/leucine
450 (SD/–Trp–Leu+His) and synthetic dropout medium lacking
451 tryptophan/leucine/histidine (SD/–Trp–Leu–His) but supplemented with 20 mM 3–
452 amino–1,2,4–triazole (3–AT) for 4 days to test the interaction.

453 **Pull–Down Assay.** The full–length *CARs* CDS were cloned into the pGEX–4T–1 and
454 transformed into *E. coli* BL21 to express GST–CAR fusion protein at 16 °C. The GST–

bioRxiv preprint doi: https://doi.org/10.1101/2021.10.13.464316; this version posted October 15, 2021. The copyright holder for this preprint (which was not certified by peer review) is the author/funder, who has granted bioRxiv a license to display the preprint in perpetuity. It is made available under aCC-BY-NC-ND 4.0 International license.

tagged CAR proteins were purified as described in the manufacturer's manual using Pierce Glutathione Agarose (16102, Thermo Fisher Scientific, USA). The 6 × His–tagged FER–CD were purified as described by[6]. Recombinant FER–CD protein was incubated overnight at 4 °C with GST beads coupled with GST–CAR in the binding buffer [50 mM Tris–HCl (pH 7.5), 150 mM NaCl, 5 mM $MgCl_2$]. The beads were washed three times with the washing buffer [50 mM Tris (pH 7.5), 150 mM NaCl, 0.1 % Triton X–100] and boiled the beads in SDS–PAGE loading buffer, and eluted proteins were analyzed by immunoblot with anti–His (M20001, Abmart) or anti–GST (SC–80998, CMC) antibody.

Bimolecular Fluorescence Complementation (BiFC) Assay. The full–length CDS of *FER* and *CARs* were cloned into plasmid pE3308 and pE3449, respectively [5]. Protoplasts were isolated from 4–week–old *Arabidopsis* rosette leaves through cellulase and macerozyme digestion for 3 hours. Then, protoplasts were co–transfected with 20 μg FER–nVenus and CAR–cCFP constructs or negative control constructs by the polyethylene glycol transformation method as previously described. The transfected protoplasts were incubated in the dark at 22 °C for 12–16 hours. Fluorescence was monitored with a confocal microscope using an excitation wavelength of 488 nm for GFP and 560 nm for FM4–64 dye (Red).

co–Immunoprecipitation (co–IP) Assay. co–IP was performed as previously described with some modifications [6]. Seven–day–old seedlings *35S::CARs–Myc* (about 0.5 g) were ground to a fine powder in liquid nitrogen and solubilized with 500 μL TBST buffer [50 mM Tris–HCl (pH 7.5), 150 mM NaCl, 5 mM $MgCl_2$, 1 mM EDTA, 1 % Triton X–100] containing 1 × protease inhibitor cocktail (78430, Thermo Fisher Scientific) and 1 × phosphatase inhibitor (78420, Thermo Fisher Scientific) and spun for 1 hour at 4 °C. The extracts were centrifuged at 16,000 g at 4 °C for 10 min, and 500 μL supernatant was transferred to incubate with prepared 20 μL Anti–Myc magnetic beads (B26301) overnight at 4 °C, and 100 μL supernatant was used as input. Then, the beads were washed 3 times with the washing buffer [50 mM Tris–HCl (pH

bioRxiv preprint doi: https://doi.org/10.1101/2021.10.13.464316; this version posted October 15, 2021. The copyright holder for this preprint (which was not certified by peer review) is the author/funder, who has granted bioRxiv a license to display the preprint in perpetuity. It is made available under aCC-BY-NC-ND 4.0 International license.

7.5), 150 mM NaCl, 0.1 % Triton X–100] containing 1 × protease inhibitor cocktail and eluted with elution buffer (0.2 M Glycine, 1 % Triton X–100, 1 mM EDTA, pH 2.5). And proteins were run on a 10 % SDS–PAGE gel and analyzed by anti–FER [5,6] and anti–Myc (CST, 2276S) antibody.

***In vitro* Phosphorylation Assay.** The phosphorylation and dephosphorylation assays were described as previously [5]. GST–CAR9 was purified by GST–beads. FER–CD–His and FER^{K565R}–CD–His (kinase dead form) were purified by Ni–beads. 1 μg recombinant proteins (GST–CAR and His–FER–CD/His–FER^{K565R}–CD) were mixed and added into reaction buffer [50 mM Tris–HCl (pH 7.5), 10 mM $MgCl_2$, 1 mM $CaCl_2$, 1 mM ATP, 1 mM DTT] to a total volume of 50 μL. The mixture was incubated at 37 °C for 30 min. The dephosphorylation assay was performed by CIP (EF0651, Thermo Fisher Scientific, USA). The reaction was stopped by adding 2 × SDS loading buffer. Proteins were separated on a 10 % SDS–PAGE gel and analyzed by anti–His or anti–GST antibody.

The ABA–induced phosphorylation co–expression system was described previously [6]. Vectors of pACYC–PYL1–FER (S–tag), pACYC–PYL1–FER^{K565R} (S–tag), and pRSF–ABI1–CAR9 (His–tag) were constructed. pRSF–ABI1–CAR9 together with pACYC–PYL1–FER (or pACYC–PYL1–FER^{K565R}) were co–transformed into one BL21 (DE3) *E. coli* strain. The transformed *E. coli* were cultured at 37 °C until the OD_{600} reached 0.6. Then, 250 μM isopropyl–β–d–thiogalactoside (IPTG) was added to induce the protein expression for 3 hours before 50 μM ABA was added to the bacterial culture to release the FER phosphorylation activity for 10 minutes. After co–expression with FER–CD or FER^{K565R}–CD, His–CAR protein was purified and then subjected to alkylation/tryptic digestion followed by liquid chromatography–tandem mass spectrometry (LC–MS/MS). For detail, 10 % SDS–PAGE gel was stained by coomassie G–250. The target bands were isolated and placed into clear tubes and digested by trypsin. Mass spectrometry was performed as described previously. Mass spectrometry was performed using LTQ–Orbitrap. Raw data were analyzed by Xcalibur v.2.1

bioRxiv preprint doi: https://doi.org/10.1101/2021.10.13.464316; this version posted October 15, 2021. The copyright holder for this preprint (which was not certified by peer review) is the author/funder, who has granted bioRxiv a license to display the preprint in perpetuity. It is made available under aCC-BY-NC-ND 4.0 International license.

(Thermo Scientific, Waltham, MA, USA) and Proteome Discoverer v.1.3 beta (Thermo Scientific, Waltham, MA, USA) (*Arabidopsis* database).

***In vivo* Phosphorylation Assay.** Phos–tag assay was performed as described previously [40]. Seven–day–old *CAR9–Myc* seedlings (about 0.1 g) were vertically grown on 1/2 MS medium which was solidified by 1.2 % agar. We added more agar in order to avoid the entrance of roots and root hairs to medium (it will hurt plant when separated them from medium). In order to avoid the disturbance of phosphorylation levels that may have been caused during removal from the solid medium. The plants on the medium were soaked by 1 μM RALF1 peptide for 10 min. After that, the plants were quickly moved in liquid nitrogen and grounded to fine powder before mixing with 70 μL 1 × SDS–PAGE loading buffer for 10 min boiling. Centrifuged at 12,000 g for 10 min and transfer the supernatant to a new tube. 10 μL supernatant was saved as input. For the detection of phosphorylated CAR proteins, 20 μL sample was separated by 10 % SDS–PAGE with 35 μM Phos–tag (WAKO, AAL–107) under lower voltage (80 v). PVDF membrane was soaked in methanol for 5 min before use, and then transferred the membrane under 100 mA for 2 h on ice (low temperature is important). The PVDF membrane was blocked with 5 % skim milk for 2 h, and then detected with anti–Myc (CST, 2276S) antibody.

For phosphorylation sites detecting *in vivo*, 2 g of *CAR–Myc* treated with or without 1 μM RALF1 for 10 min as described above. Total protein was extracted by using 0.5 mL of NEB buffer [20 mM Hepes–KOH (pH 7.5), 40 mM KCl, 1 mM EDTA, 1 mM PMSF, 1 % protease inhibitor mixture (Thermo Fisher Scientific, 78420), and 1 % phosphatase inhibitors (Bimake, B15001)]. The homogenized sample was centrifuged at 12,000 g for 10 min each at 4 °C. Then, 20 μL prepared anti–Myc magnetic beads (B26301) for each sample was used to immunoprecipitate CAR–Myc protein complexes at 4 °C for 5 hours. The beads were washed three times in washing buffer [20 mM Hepes–KOH (pH 7.5), 40 mM KCl, and 0.1 % Triton X–100] at 4 °C. The beads were resuspended in 30 μL of 1 × SDS loading buffer, boiled for 10 min,

bioRxiv preprint doi: https://doi.org/10.1101/2021.10.13.464316; this version posted October 15, 2021. The copyright holder for this preprint (which was not certified by peer review) is the author/funder, who has granted bioRxiv a license to display the preprint in perpetuity. It is made available under aCC-BY-NC-ND 4.0 International license.

separated by 10 % (w/v) SDS–PAGE gel. The CAR–Myc bands digested, and analyzed by MS as described previously.

Pan–anti–CARs Antibody Production. Antibody production was performed as previous study[6]. This antibody is raised by using full–length CAR9 expressed and purified from *E.coil* BL21. A 1–month–old ICR mouse (SLAC laboratory animal) was injected with 50 μg GST–CAR9 protein emulsified with Complete Freund's adjuvant (F5881, Sigma–Aldrich). Two weeks later, 50 μg GST–CAR9 protein emulsified with Incomplete Freund's adjuvant (F5506, Sigma–Aldrich) was injected into the ICR mouse and then once again in the next week. The serum of the immunized mouse was obtained as antibody for immunoblot detection. We tested the antibody in WT, *car9*, *3M* and *5M* mutant lines by an immunoblot. Because of ten CAR family members share common motif and sequence, we still detected homologs in CAR9 signal mutants using this antibody, but this interacted band will be sharply reduced when using in CARs multiple mutants. Thus, we named this antibody as pan–anti–CARs antibody.

Lipid Binding Assay. Phospholipid binding to proteins was assessed as described [31]. Briefly, phosphatidylserine (PS): phosphatidylcholine (PC) (25:75) was prepared in chloroform and dried to obtain a thin layer under a stream of nitrogen. The dried lipids were resuspended in buffer A (100 mM NaCl, 50 mM HEPES, pH 6.8) and mixed by vortexing for 20 min. Large multilamellar vesicles were obtained by centrifugation at 16,000 g for 20 min. Resuspended the vesicles in 1 mL of buffer A with multiple concentrations of free Ca^{2+} and stored at 4 °C. The vesicles (about 100 μg of phospholipids) were mixed with the different forms of GST–CAR9 (5 μg). The mixture was incubated with or without 1 mM Ca^{2+} via gentle shaking (250 rpm) for 30 min at room temperature. The vesicles and the bound proteins were pelleted by centrifugation at 12,000 g at 4 °C for 10 min and washed twice with 0.5 mL of buffer A. Samples were boiled with 1 × protein loading buffer for 10 min and separated by 10 % SDS–PAGE. Proteins were revealed by using anti–GST antibody.

bioRxiv preprint doi: https://doi.org/10.1101/2021.10.13.464316; this version posted October 15, 2021. The copyright holder for this preprint (which was not certified by peer review) is the author/funder, who has granted bioRxiv a license to display the preprint in perpetuity. It is made available under aCC-BY-NC-ND 4.0 International license.

Polysome Profiling Assay and Real–Time PCR. Arabidopsis polysomes profiling assay was performed as described [12,51]. Briefly, 7–day–old seedlings (about 0.5 g) were treated with RALF1 (1 μM) for 10 min and then ground in liquid nitrogen followed by resuspension in polysome extraction buffer. Supernatant was loaded onto a 15 %–60 % sucrose gradient and spun in a Beckman SW 32 Ti rotor at 170,000 g for 4 h at 4 °C. We manually collected 11 fractions. Then, isolated the RNA from the last four fractions by RNAiso plus (Takara) kit. RT–qPCR analysis was used to quantify the total target relative transcript content in the input and the relative content of target transcripts associated with heavier polysomes in the bottom four fractions. Primers for RT–qPCR is shown in Table S1. ACTIN as a reference gene to detect the RNA levels of CARs.

ROS Burst Assay. The flg22–induced ROS burst measurement assay was performed as previously described [8]. Four–week–old *Arabidopsis* rosette leaves were cut into pieces (4 mm in diameter) and collected in 96–well plates containing sterile water (pH 5.8) and recovered overnight in dark at 22 °C. After 24 hours, sterile water was replaced by a reaction solution [20 μm/L luminol L–012 (Sigma–Aldrich), 1 μg/mL horseradish peroxidase (HRP, Sigma Aldrich), 0.1 μm/L flg22] with or without 1 μM RALF1 (RALF1 elution buffer as a negative control). Luminescence was measured for the indicated time period using Fluoroskan Ascent FL (Thermo Scientific). For the MβCD treatment, we first prepared 10 mM MβCD solution (1.331 g powder dissolved in 100 ml sterile water, pH 5.8) (Solarbio, M9040) and pretreated sample for 30 min. Next, we replaced the MβCD solution with reaction solution and the following steps were as previously described. ROS production was displayed as either the progression of photon counts or the integration of total photon counts. There were three replicates of every sample. Values are means of the total photon counts inhibition over 25 min ± SD. We exported the original data from Fluoroskan Ascent FL and processed data through GraphPad Prism software.

Fluorescence Recovery after Photobleaching (FRAP) Analysis. The FRAP assay was performed in the root of *GFP–Folt1* and *GFP–Folt1/fer–4* [36]. Samples were

bioRxiv preprint doi: https://doi.org/10.1101/2021.10.13.464316; this version posted October 15, 2021. The copyright holder for this preprint (which was not certified by peer review) is the author/funder, who has granted bioRxiv a license to display the preprint in perpetuity. It is made available under aCC-BY-NC-ND 4.0 International license.

pretreated with RALF1 (1 μM) or RALF23 (1 μM) for 10 min, the water as negative control. FRAP was imaged with a Zeiss LSM 880 confocal laser scanning microscope (excitation at 488 nm, emission 500–570 nm, × 63 oil lens). Rectangular region of interest (ROIs) (4 × 4 μm) was bleached in median optical sections of the PM. ROIs were bleached with 100 % laser power at 488 nm, and 60 % fluorescence was set to be bleached. Then the fluorescence recovery was monitored every 1 s within total 3 min. Fluorescence intensity data were normalized using the equation: $I_n = [(I_t – I_{min}) / (I_{max} – I_{min})]$ [46]. I_n, the normalized intensity; I_t, the intensity at any time; I_{min}, the minimum intensity post–photobleaching; I_{max}, the mean intensity before photobleaching.

Variable–Angle Total Internal Reflection Fluorescence Microscopy (VA–TIRFM) Imaging. VA–TIRFM was performed as previously described[34]. Four–day–old *GFP–Flot1*[34] and GFP–Flot1/*fer–4* seedlings were used in this experiment. The *GFP–Flot1* was treated with RALF1 (1 μM) for 10 min in the liquid 1/2MS before observation. For observation, seedlings were softly transferred onto a glass slide and soaked with liquid 1/2 MS, then covered with a coverslip. A custom–built VA–TIRFM based on an Olympus IX–71 microscope equipped with a total internal reflective fluorescence illuminator and a 100 × oil–immersion objective (numerical aperture of 1.45, Olympus) was used here. The 473 nm laser line from a diode laser was used to excite GFP. The emission fluorescence signals were detected with a back–illuminated EM–CCD camera (ANDOR iXon DV8897D–CS0–VP; And / or Technology, Belfast, UK) after filtering with band–pass filters. The gain of the EMCCD camera was set to 300 throughout all single–molecule imaging experiments; the setting was in the linear dynamic range of the EMCCD camera. Images were acquired with an exposure time of 100 mS and analyzed with Image J. Gauss fit curve were calculated by the Origin 8 software.

Lipid Staining. For di–4–ANEPPDHQ lipid staining, four–day–old seedlings are collected for each genotype. 5 μM (work concentration) di–4–ANEPPDHQ (Thermo Fisher, D36802) was added to the liquid 1/2 MS medium for 5 min staining, then washing 3 times using liquid 1/2 MS medium. The seedlings were observed on the Zeiss

bioRxiv preprint doi: https://doi.org/10.1101/2021.10.13.464316; this version posted October 15, 2021. The copyright holder for this preprint (which was not certified by peer review) is the author/funder, who has granted bioRxiv a license to display the preprint in perpetuity. It is made available under aCC-BY-NC-ND 4.0 International license.

LSM 880 (Alpha Plan Apochromat 63 ×, NA 1.4 oil objective). Quantification of lipid polarity in root cell meristematic zone has been described previously [28,37]. Briefly, the di–4–ANEPPDHQ fluorescence signal was excited at 488 nm, the membrane order phase was recorded in the range of 500 – 580 nm, the membrane disorder phase was recorded in the range of 620 – 750 nm. The signal of di–4–ANEPPDHQ staining was quantified by ImageJ. For the quantification, both ordered (500 – 580 nm) and disordered (620 – 750 nm) phase fluorescence images are designated as ch00 and ch01, respectively. The GP (Generalized Polarization) value, which is positively correlated with the degree of membrane lipid order, was obtained by calculating mean value of all effective pixels recorded in each region of interest (ROI) of the image. The analysis threshold is fixed at 15, the color scale of the output GP image is set to "16 colors", and no immunofluorescence mask was selected. After processing, manually select the ROI from the GP image for further calculation of the average GP value. More than 40 ROIs were selected from at least 6 images of each process to generate average GP value. The representative images in this work showed a “merge” image and a “HSB” image. “Merge” is merged of the green (500 – 580 nm) and red (620 – 750 nm) emission channels from di–4–ANEPPDHQ. “HSB” (hue–saturation–brightness) picture, a GP image with radiation color coding. The GP value is specified as hue (color) and the average intensity is set as brightness.

***Pto* DC3000 infection assay.** For *Pto* DC3000 infection assay[8], *Pseudomonas syringae pv. Tomato (Pto)* DC3000 strains were grown overnight in King’s B medium (10 g/L proteose peptone, 1.5 g/L anhydrous K2HPO4, 5 g/L MgSO4) with shaking at 28°C. Bacteria were collected and resuspended in 10 mM $MgCl_2$ at OD_{600} = 0.02. 4-week-old *Arabidopsis* were allowed to permeate the 4th and 5th rosette leaves under pressure. After infection, the plants were moved to plant incubator with a relative humidity of 80% at 22 °C, and allowed to grow for three days. Three leaf discs per sample from different plants were collected in microfuge tubes and ground with a drill-adapted pestle. Serial dilutions were plated on LB agar and colonies were counted after two days of cultivation at 28 °C.

bioRxiv preprint doi: https://doi.org/10.1101/2021.10.13.464316; this version posted October 15, 2021. The copyright holder for this preprint (which was not certified by peer review) is the author/funder, who has granted bioRxiv a license to display the preprint in perpetuity. It is made available under aCC-BY-NC-ND 4.0 International license.

Statistical Analysis. Software SPSS Statistics 17.0 was used. Data are shown as mean ± s.d.; * $p < 0.05$, ** $p < 0.01$, *** $p < 0.001$; n.s., not significant. One–way ANOVA with Tukey's test were used as mention in figure note.

Data availability: The data that support the findings of this study are available from the corresponding author upon reasonable request.

Acknowledgments: We thank Liming Xiong, Tao Qin, and Chao Li for providing plant materials and Cyril Zipfel for critical comments and suggestions. This work was supported by grants from National Natural Science Foundation of China (NSFC–31871396, 31571444), Young Elite Scientist Sponsorship program of CAST (YESS20160001), and the Open Research Fund of the State Key Laboratory of Hybrid Rice (Hunan Hybrid Rice Research Center) to F.Y. Work in P.L.R. laboratory was funded by grant BIO2017-82503-R.

Author Contributions: S.R.Z, F.Y., and W.J.C. conceived the project and designed the research; W.J.C., H.N.Z., S.R.Z., F.X., M.Y., G.Y.X., J.C. A.C., L.R., Y.Q.L, Q.J.X., Q.F., and L.L. performed the research; D.S.W., X.S.L., A.C., S.J.D., X.J.L, and P.L.R. contributed new reagents/analytic tools; F.Y., S.R.Z and W.J.C analyzed data and wrote the paper with contribution from P.L.R. and Y. J.; all authors reviewed and approved the manuscript for publication.

Competing Interests: The authors declare no competing financial interests.

bioRxiv preprint doi: https://doi.org/10.1101/2021.10.13.464316; this version posted October 15, 2021. The copyright holder for this preprint (which was not certified by peer review) is the author/funder, who has granted bioRxiv a license to display the preprint in perpetuity. It is made available under aCC-BY-NC-ND 4.0 International license.

References

1. Escobar-Restrepo, J.M., *et al.* The FERONIA receptor-like kinase mediates male-female interactions during pollen tube reception. *Science* **317**, 656-660 (2007).
2. Li, C., *et al.* Glycosylphosphatidylinositol-anchored proteins as chaperones and co-receptors for FERONIA receptor kinase signaling in Arabidopsis. *Elife* **4**, e06587 (2015).
3. Guo, H., *et al.* Three related receptor-like kinases are required for optimal cell elongation in Arabidopsis thaliana. *Proceedings of the National Academy of Sciences* **106**, 7648-7653 (2009).
4. Duan, Q., Kita, D., Li, C., Cheung, A.Y. & Wu, H.-M. FERONIA receptor-like kinase regulates RHO GTPase signaling of root hair development. *Proceedings of the National Academy of Sciences* **107**, 17821-17826 (2010).
5. Du, C., *et al.* Receptor kinase complex transmits RALF peptide signal to inhibit root growth in Arabidopsis. *Proceedings of the National Academy of Sciences* **113**, E8326-E8334 (2016).
6. Li, C., *et al.* EBP1 nuclear accumulation negatively feeds back on FERONIA-mediated RALF1 signaling. *PLoS Biol* **16**, e2006340 (2018).
7. Chen, J., *et al.* FERONIA interacts with ABI2-type phosphatases to facilitate signaling cross-talk between abscisic acid and RALF peptide in Arabidopsis. *Proc Natl Acad Sci U S A* **113**, E5519-5527 (2016).
8. Stegmann, M., *et al.* The receptor kinase FER is a RALF-regulated scaffold controlling plant immune signaling. *Science* **355**, 287-289 (2017).
9. Yang, T., *et al.* Receptor protein kinase FERONIA controls leaf starch accumulation by interacting with glyceraldehyde-3-phosphate dehydrogenase. *Biochemical and biophysical research communications* **465**, 77-82 (2015).
10. Xu, G., *et al.* FERONIA phosphorylates E3 ubiquitin ligase ATL6 to modulate the stability of 14-3-3 proteins in response to the carbon/nitrogen ratio. *J Exp Bot* **70**, 6375-6388 (2019).
11. Wang, L., *et al.* RALF1-FERONIA complex affects splicing dynamics to modulate stress responses and growth in plants. *Science advances* **6**, eaaz1622 (2020).
12. Zhu, S., *et al.* The RALF1–FERONIA complex phosphorylates eIF4E1 to promote protein synthesis and polar root hair growth. *Mol Plant* (2020).
13. Xiao, Y., *et al.* Mechanisms of RALF peptide perception by a heterotypic receptor complex. *Nature* **572**, 270-274 (2019).
14. Spira, F., *et al.* Patchwork organization of the yeast plasma membrane into numerous coexisting domains. *Nat Cell Biol* **14**, 640-648 (2012).
15. Jarsch, I.K., *et al.* Plasma Membranes Are Subcompartmentalized into a Plethora of Coexisting and Diverse Microdomains in Arabidopsis and Nicotiana benthamiana. *Plant Cell* **26**, 1698-1711 (2014).
16. Jaillais, Y. & Ott, T. The Nanoscale Organization of the Plasma Membrane and Its Importance in Signaling: A Proteolipid Perspective. *Plant Physiol* **182**, 1682-1696 (2020).
17. Ott, T. Membrane nanodomains and microdomains in plant-microbe interactions. *Curr Opin Plant Biol* **40**, 82-88 (2017).
18. Garcia-Parajo, M.F., Cambi, A., Torreno-Pina, J.A., Thompson, N. & Jacobson, K. Nanoclustering as a dominant feature of plasma membrane organization. *J Cell Sci* **127**, 4995-5005 (2014).
19. Sezgin, E., Levental, I., Mayor, S. & Eggeling, C. The mystery of membrane organization:

bioRxiv preprint doi: https://doi.org/10.1101/2021.10.13.464316; this version posted October 15, 2021. The copyright holder for this preprint (which was not certified by peer review) is the author/funder, who has granted bioRxiv a license to display the preprint in perpetuity. It is made available under aCC-BY-NC-ND 4.0 International license.

composition, regulation and roles of lipid rafts. *Nat Rev Mol Cell Biol* **18**, 361-374 (2017).

20. Pan, X., *et al.* Auxin-induced signaling protein nanoclustering contributes to cell polarity formation. *Nat Commun* **11**, 3914 (2020).
21. Simons, K. & Gerl, M.J. Revitalizing membrane rafts: new tools and insights. *Nature Reviews Molecular Cell Biology* **11**, 688-699 (2010).
22. Burkart, R.C. & Stahl, Y. Dynamic complexity: plant receptor complexes at the plasma membrane. *Curr Opin Plant Biol* **40**, 15-21 (2017).
23. Platre, M.P., *et al.* Developmental control of plant Rho GTPase nano-organization by the lipid phosphatidylserine. *science* **364**, 57-62 (2019).
24. Gronnier, J., Gerbeau-Pissot, P., Germain, V., Mongrand, S. & Simon-Plas, F. Divide and Rule: Plant Plasma Membrane Organization. *Trends Plant Sci* **23**, 899-917 (2018).
25. Smokvarska, M., Jaillais, Y. & Martiniere, A. Function of membrane domains in rho-of-plant signaling. *Plant Physiol* **185**, 663-681 (2021).
26. Demir, F., *et al.* Arabidopsis nanodomain-delimited ABA signaling pathway regulates the anion channel SLAH3. *Proceedings of the National Academy of Sciences* **110**, 8296-8301 (2013).
27. Wang, L., *et al.* Spatiotemporal Dynamics of the BRI1 Receptor and its Regulation by Membrane Microdomains in Living Arabidopsis Cells. *Mol Plant* **8**, 1334-1349 (2015).
28. Huang, D., *et al.* Salicylic acid-mediated plasmodesmal closure via Remorin-dependent lipid organization. *Proc Natl Acad Sci U S A* **116**, 21274-21284 (2019).
29. Bucherl, C.A., *et al.* Plant immune and growth receptors share common signalling components but localise to distinct plasma membrane nanodomains. *Elife* **6**(2017).
30. Diaz, M., *et al.* Calcium-dependent oligomerization of CAR proteins at cell membrane modulates ABA signaling. *Proc Natl Acad Sci U S A* **113**, E396-405 (2016).
31. Rodriguez, L., *et al.* C2-domain abscisic acid-related proteins mediate the interaction of PYR/PYL/RCAR abscisic acid receptors with the plasma membrane and regulate abscisic acid sensitivity in Arabidopsis. *Plant Cell* **26**, 4802-4820 (2014).
32. Martens, S. & McMahon, H.T. Mechanisms of membrane fusion: disparate players and common principles. *Nat Rev Mol Cell Biol* **9**, 543-556 (2008).
33. Morrow, I.C., *et al.* Flotillin-1/reggie-2 traffics to surface raft domains via a novel golgi-independent pathway. Identification of a novel membrane targeting domain and a role for palmitoylation. *J Biol Chem* **277**, 48834-48841 (2002).
34. Li, R., *et al.* A membrane microdomain-associated protein, Arabidopsis Flot1, is involved in a clathrin-independent endocytic pathway and is required for seedling development. *Plant Cell* **24**, 2105-2122 (2012).
35. Yu, M., *et al.* The RALF1-FERONIA interaction modulates endocytosis to mediate control of root growth in Arabidopsis. *Development*, dev.189902 (2020).
36. Luu, D.T., Martiniere, A., Sorieul, M., Runions, J. & Maurel, C. Fluorescence recovery after photobleaching reveals high cycling dynamics of plasma membrane aquaporins in Arabidopsis roots under salt stress. *The Plant Journal* **69**, 894-905 (2012).
37. Owen, D.M., Rentero, C., Magenau, A., Abu-Siniyeh, A. & Gaus, K. Quantitative imaging of membrane lipid order in cells and organisms. *Nat Protoc* **7**, 24-35 (2011).
38. Gronnier, J., *et al.* FERONIA regulates FLS2 plasma membrane nanoscale dynamics to modulate plant immune signaling. *bioRxiv*, 2020.2007.2020.212233 (2020).
39. Qin, T., Tian, Q., Wang, G. & Xiong, L. LOWER TEMPERATURE 1 Enhances ABA Responses

bioRxiv preprint doi: https://doi.org/10.1101/2021.10.13.464316; this version posted October 15, 2021. The copyright holder for this preprint (which was not certified by peer review) is the author/funder, who has granted bioRxiv a license to display the preprint in perpetuity. It is made available under aCC-BY-NC-ND 4.0 International license.

and Plant Drought Tolerance by Modulating the Stability and Localization of C2-Domain ABA-Related Proteins in Arabidopsis. *Mol Plant* **12**, 1243-1258 (2019).

40. Chen, G.H., Liu, M.J., Xiong, Y., Sheen, J. & Wu, S.H. TOR and RPS6 transmit light signals to enhance protein translation in deetiolating Arabidopsis seedlings. *Proc Natl Acad Sci U S A* **115**, 12823-12828 (2018).

41. Zhou, Y.B., *et al.* The Receptor-Like Cytoplasmic Kinase STRK1 Phosphorylates and Activates CatC, Thereby Regulating H2O2 Homeostasis and Improving Salt Tolerance in Rice. *Plant Cell* **30**, 1100-1118 (2018).

42. Ngo, Q.A., Vogler, H., Lituiev, D., Nestorova, A. & Grossniklaus, U.J.D.C. A calcium dialog mediated by the FERONIA Signal transduction pathway controls plant sperm delivery. *Developmental Cell* **29**, 491-500 (2014).

43. Simon, M.L., *et al.* A PtdIns(4)P-driven electrostatic field controls cell membrane identity and signalling in plants. *Nat Plants* **2**, 16089 (2016).

44. Platre, M.P., *et al.* A Combinatorial Lipid Code Shapes the Electrostatic Landscape of Plant Endomembranes. *Dev Cell* **45**, 465-480 e411 (2018).

45. Zhang, X., Yang, Z., Wu, D. & Yu, F. RALF–FERONIA Signaling: Linking Plant Immune Response with Cell Growth. *Plant Communications* **1**(2020).

46. Martiniere, A., *et al.* Cell wall constrains lateral diffusion of plant plasma-membrane proteins. *Proceedings of the National Academy of Sciences* **109**, 12805-12810 (2012).

47. McKenna, J.F., *et al.* The cell wall regulates dynamics and size of plasma-membrane nanodomains in Arabidopsis. *Proc Natl Acad Sci U S A* **116**, 12857-12862 (2019).

48. Danek, M., *et al.* Cell wall contributes to the stability of plasma membrane nanodomain organization of Arabidopsis thaliana FLOTILLIN2 and HYPERSENSITIVE INDUCED REACTION1 proteins. *Plant J* **101**, 619-636 (2020).

49. Zhu, S., Fu, Q., Xu, F., Zheng, H. & Yu, F. New paradigms in cell adaptation: decades of discoveries on the CrRLK1L receptor kinase signalling network. *New Phytol* (2021).

50. Du, C., *et al.* Receptor kinase complex transmits RALF peptide signal to inhibit root growth in Arabidopsis. *Proc Natl Acad Sci U S A* **113**, E8326-E8334 (2016).

51. Missra, A. & Von Arnim, A.G. Analysis of mRNA Translation States in Arabidopsis Over the Diurnal Cycle by Polysome Microarray. *Methods of Molecular Biology* **1158**, 157-174 (2014).

bioRxiv preprint doi: https://doi.org/10.1101/2021.10.13.464316; this version posted October 15, 2021. The copyright holder for this preprint (which was not certified by peer review) is the author/funder, who has granted bioRxiv a license to display the preprint in perpetuity. It is made available under aCC-BY-NC-ND 4.0 International license.

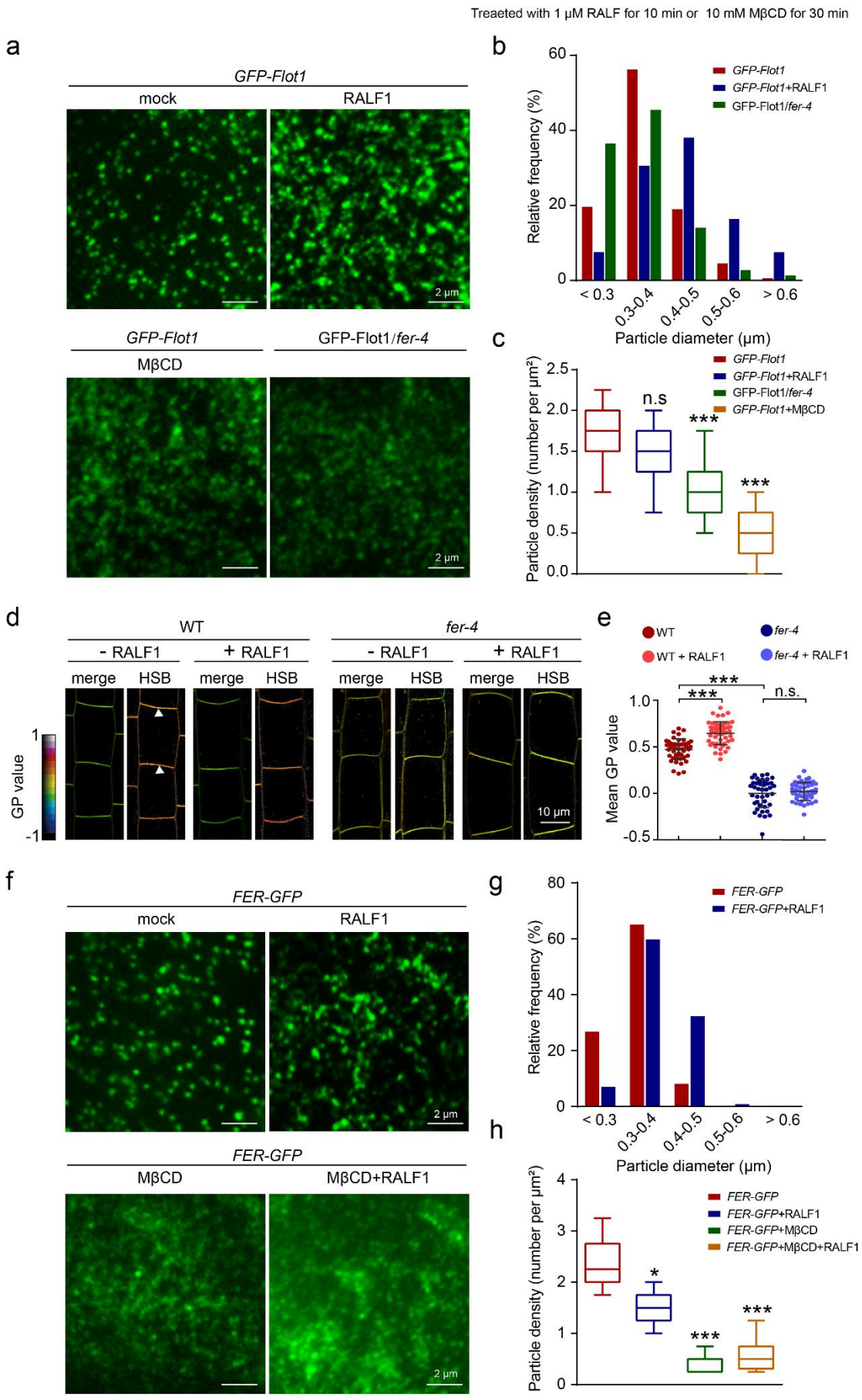

789

bioRxiv preprint doi: https://doi.org/10.1101/2021.10.13.464316; this version posted October 15, 2021. The copyright holder for this preprint (which was not certified by peer review) is the author/funder, who has granted bioRxiv a license to display the preprint in perpetuity. It is made available under aCC-BY-NC-ND 4.0 International license.

Fig. 1. RALF1 promotes the formation of FER and Flot1 nanoclusters and ordered lipid. (**a**) VA-TIRFM images of GFP-Flot1 at the PM in root cells with or without RALF1 (1 μM, 10 min) or MβCD (10 mM, 30 min) treatment in WT and *fer-4* background. (**b**) Histogram of GFP-Flot1 particle size distribution in WT, RALF1-treated, and *fer-4* background. (**c**) Quantitative comparison of GFP-Flot1 particle density in different treatments. (**d**) Di–4–ANEPPDHQ lipid staining assay of WT and *fer–4* root meristematic cells with or without RALF1 treatment. The GP value is indicated with a colored box. (**e**) Statistical analysis of the GP value in (d). The white triangle in (d) indicates the regions for GP value quantification. For each treatment, 42 – 51 cells from 5 roots were measured. (**f**) VA-TIRFM images of FER-GFP at the PM in root cells with or without RALF1 (1 μM, 10 min) or MβCD (10 mM, 30 min) treatment in WT background. (**g**) Histogram of FER-GFP particle size distribution in WT and RALF1-treated. (**h**) Quantitative comparison of FER-GFP particle density in different treatments.

Three biological replicates were performed with similar results. Data are shown as the mean ± s.d., *$p < 0.05$, ***$p < 0.001$, and n.s., not significant. One–way ANOVA with Tukey's test.

bioRxiv preprint doi: https://doi.org/10.1101/2021.10.13.464316; this version posted October 15, 2021. The copyright holder for this preprint (which was not certified by peer review) is the author/funder, who has granted bioRxiv a license to display the preprint in perpetuity. It is made available under aCC-BY-NC-ND 4.0 International license.

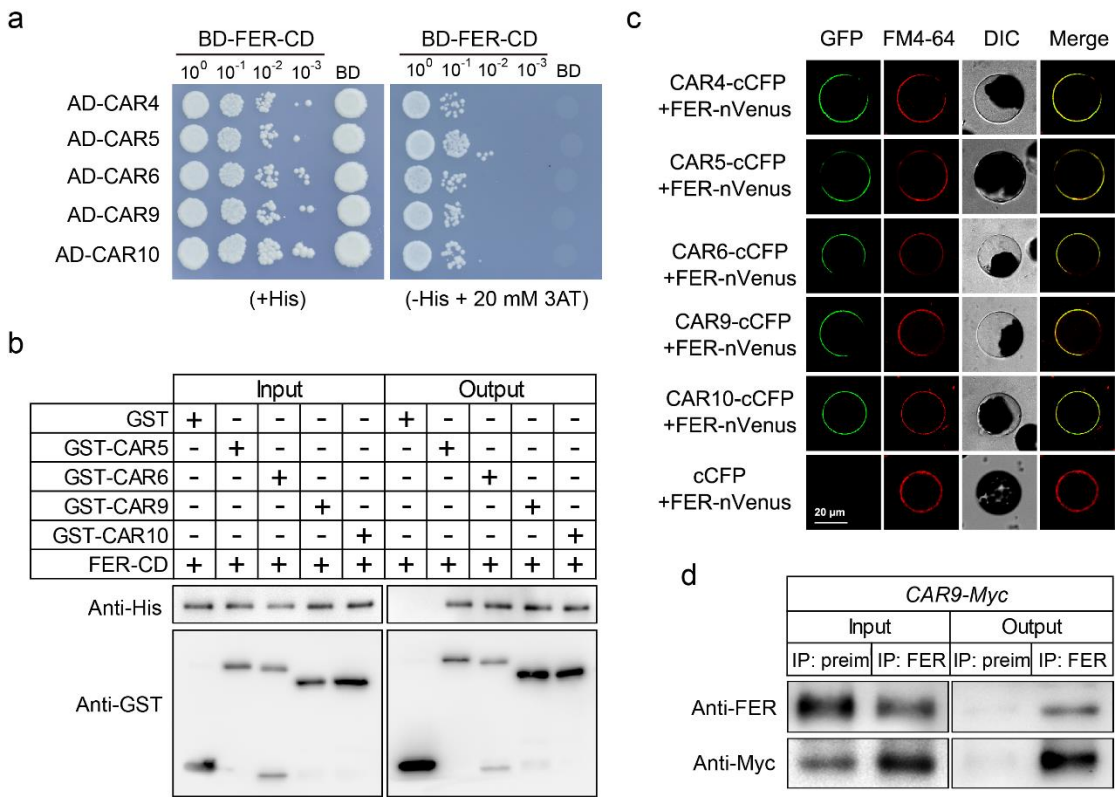

Fig. 2. FER physically interacts with CARs. (**a**) Y2H assays showing the interaction between CARs and FER. SD (–His/–Leu/–Trp) selection medium containing 20 mM 3–AT was used to test the interaction. The CAR members were cloned into the pGADT7 (AD) vector, and the FER-CD was cloned into the pGBKT7 (BD) vector. (**b**) GST pull–down assay. The indicated GST–tag and His–tag were detected by anti–GST and anti–His, respectively. (**c**) FER interacts with CARs in BiFC assays in *Arabidopsis* protoplasts. Negative control (cCFP + FER–Venus) are shown, and FM4–64 indicates the PM (red). (**d**) Co–IP assays. The immunoprecipitated FER and coimmunoprecipitated CAR9 were indicated using anti–FER and anti–Myc antibodies, respectively. Preimmune serum ("Preim") was used as negative control.

At least three biological replicates of (a) – (d) were performed with similar results.

bioRxiv preprint doi: https://doi.org/10.1101/2021.10.13.464316; this version posted October 15, 2021. The copyright holder for this preprint (which was not certified by peer review) is the author/funder, who has granted bioRxiv a license to display the preprint in perpetuity. It is made available under aCC-BY-NC-ND 4.0 International license.

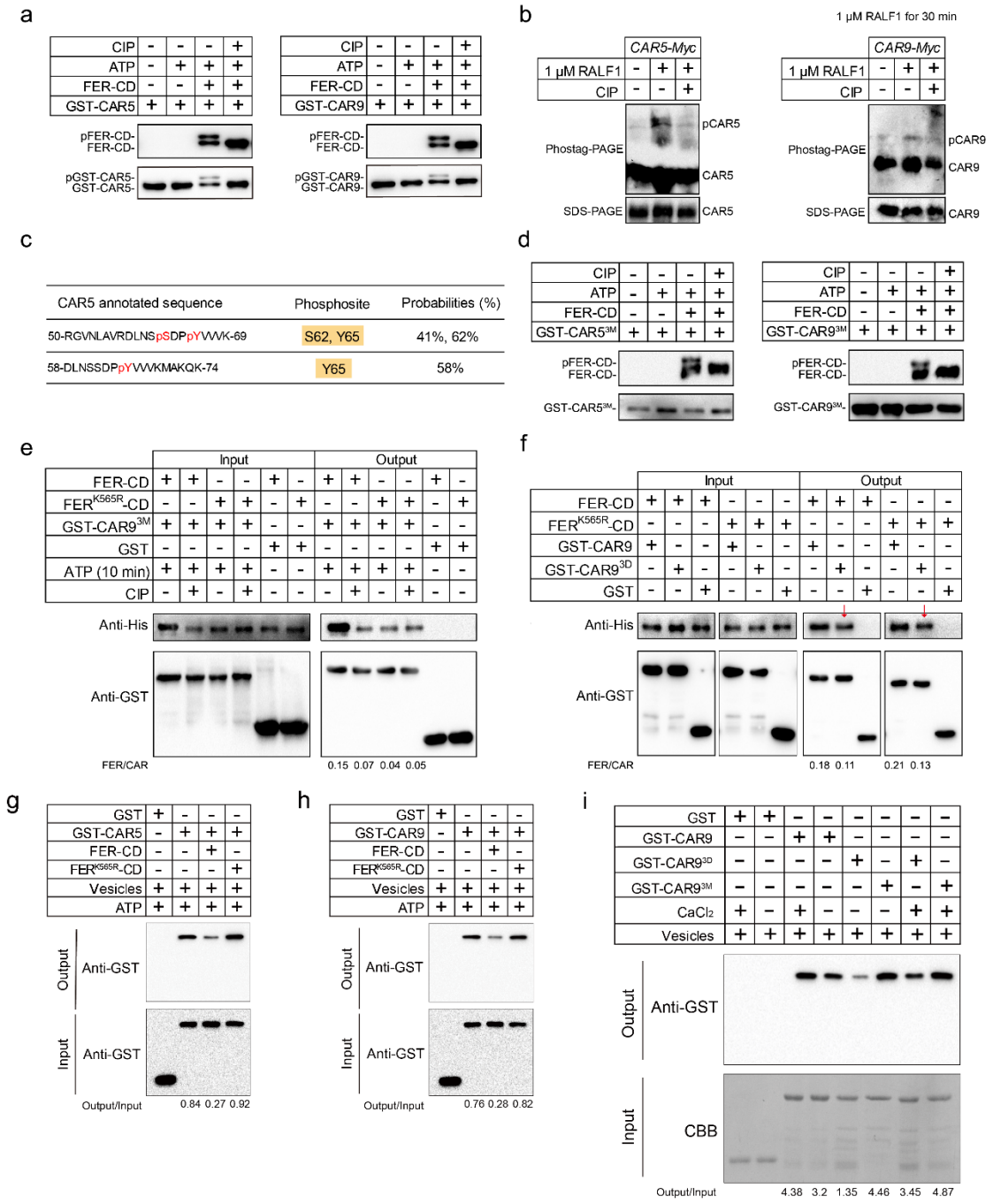

Fig. 3. RALF1–FER phosphorylates CAR proteins and further regulates the interaction of CAR proteins and anionic lipid. (**a**) *In vitro* phosphorylation assays showing that FER–CD can phosphorylate GST–CAR5 and GST–CAR9, as detected using anti–GST and anti–His antibodies. (**b**) Phostag–PAGE assays *in vivo*. Phosphorylated CAR5–Myc and CAR9–Myc bands are indicated as pCAR5–Myc and pCAR9–Myc. (**c**) Examples of phosphopeptides of CAR5 *in vivo*. The maximum probability shown for each phosphorylation site was calculated by the Andromeda

bioRxiv preprint doi: https://doi.org/10.1101/2021.10.13.464316; this version posted October 15, 2021. The copyright holder for this preprint (which was not certified by peer review) is the author/funder, who has granted bioRxiv a license to display the preprint in perpetuity. It is made available under aCC-BY-NC-ND 4.0 International license.

algorithm integrated in MaxQuant. (**d**) *In vitro* phosphorylation assays showing that GST–CAR5^{3M} and GST–CAR9^{3M} were not phosphorylated by FER–CD. (**e**) GST pull–down assay showing that phosphorylated FER–CD exhibits a higher affinity towards GST–CAR9^{3M}. The relative protein intensity of FER–CD–His and FER^{K565R}–CD–His in the output was analyzed using ImageJ. (**f**) GST pull–down assay. GST–CAR9^{3D} shows a weaker interaction with FER–CD–His and FER^{K565R}–CD–His. The relative protein intensity of FER–CD–His and FER^{K565R}–CD–His in the output was analyzed using ImageJ. The red arrow pointing the weakened anti-His panel. (**g-h**) Phosphorylated CAR5 and CAR9 (0.1 μM) show weaker lipid binding ability in the presence of 1 mM $CaCl_2$. (**i**) Lipid binding abilities of three forms of CAR9 in the presence or absence of 1 mM $CaCl_2$. Immunoblot assays showing the protein levels by ImageJ.

At least three biological replicates were performed with similar results.

bioRxiv preprint doi: https://doi.org/10.1101/2021.10.13.464316; this version posted October 15, 2021. The copyright holder for this preprint (which was not certified by peer review) is the author/funder, who has granted bioRxiv a license to display the preprint in perpetuity. It is made available under aCC-BY-NC-ND 4.0 International license.

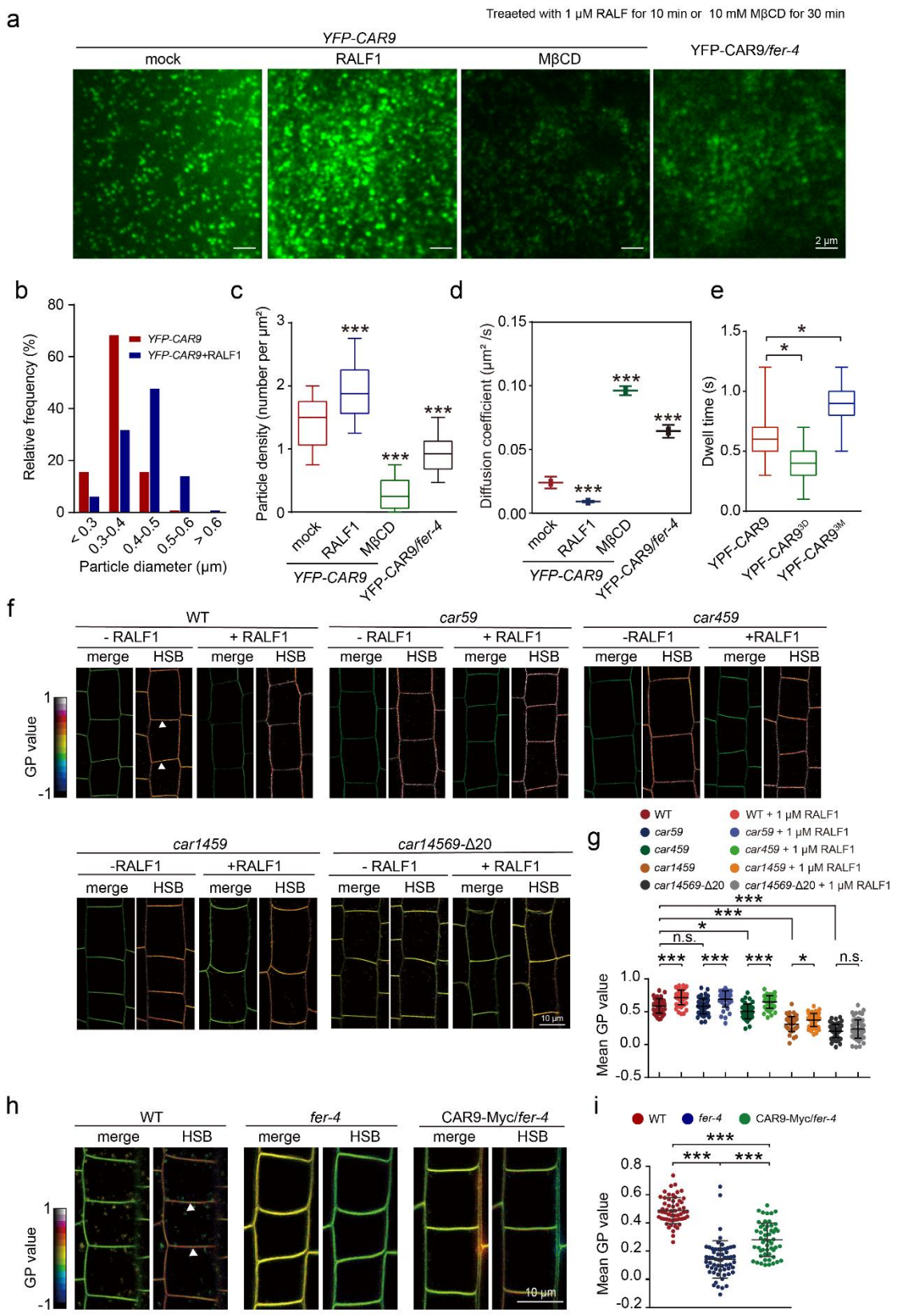

841

842 **Fig. 4. RALF1-induced nanoclustering of CAR9 and CARs are required for lipid**

843 **ordered phase formation.** (**a**) VA-TIRFM images of YFP-CAR9 at the PM in root

bioRxiv preprint doi: https://doi.org/10.1101/2021.10.13.464316; this version posted October 15, 2021. The copyright holder for this preprint (which was not certified by peer review) is the author/funder, who has granted bioRxiv a license to display the preprint in perpetuity. It is made available under aCC-BY-NC-ND 4.0 International license.

cells with or without RALF1 (1 μM, 10 min) or MβCD (10 mM, 30 min) treatment in WT and *fer-4* background. (**b**) Histogram of YFP-CAR9 particle size distribution in WT background. (**c**) Quantitative comparison of YFP-CAR9 particle density in different groups. (**d**) Comparison of diffusion coefficients of YFP-CAR9 particles in different groups. 4-day-old seedlings were treated by RALF1 or MβCD. The number of particles analyzed in each treatment are more than 3000 spots. **(e)** Dwell time was analyzed under YFP-CAR9, YFP-CAR9^{3D}, and YFP-CAR9^{3M} background. (**f**) Di–4–ANEPPDHQ lipid staining assay in root cells of *car59*, *car459*, *car1459* and *car14569*–Δ20. The GP value is indicated with a colored box. (**g**) Statistical analysis of the GP value in (f). The white triangle in (f) indicates the regions for GP value quantification. For each treatment, 41 – 60 cells from 5 roots were measured. (**h**) Di–4–ANEPPDHQ lipid staining assay of WT, *fer–4*, and CAR9–Myc/*fer–4*. The GP value was indicated with a colored box. (**i**) Statistical analysis of the GP value in (h). The white triangle in (h) indicated the regions for GP value quantification. For each treatment, 41–50 cells from 5 roots were measured.

At least three biological replicates were performed with similar results. Data are shown as the mean ± s.d., *$p < 0.05$, ***$p < 0.001$, n.s., not significant. One–way ANOVA with Tukey's test.

bioRxiv preprint doi: https://doi.org/10.1101/2021.10.13.464316; this version posted October 15, 2021. The copyright holder for this preprint (which was not certified by peer review) is the author/funder, who has granted bioRxiv a license to display the preprint in perpetuity. It is made available under aCC-BY-NC-ND 4.0 International license.

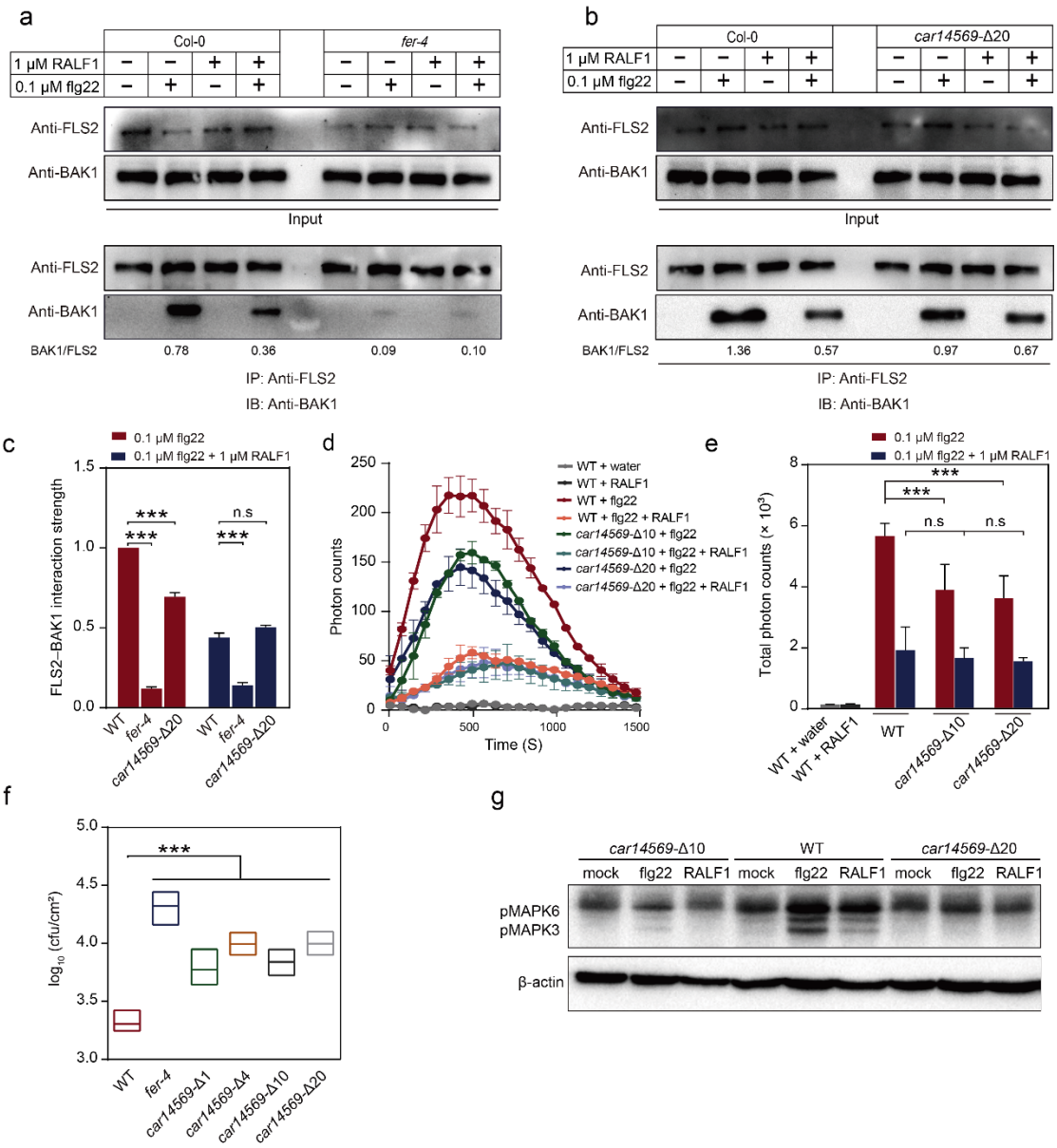

Fig. 5. RALF-FER-CAR axis as a signal platform to integrate immunity response. (**a-b**) Co–IP assay showing the weaker interaction between FLS2 and BAK1 in *fer–4* and *car14569*–Δ20 with or without RALF1 and flg22 treatment for 10 min. Western blots were probed with anti–FLS2 and anti–BAK1 antibodies. The relative protein intensity of FLS2 and BAK1 was analyzed using Image J. (**c**) Quantitative comparison of FLS2 and BAK1 interaction strength in (a) and (b). The ratio of BAK1 to FLS2 in (a) and (b) were normalized. (**d-e**) The ROS burst was measured after elicitation of leaf discs from the indicated mutant lines with 0.1 μM flg22 and/or 1 μM RALF1 in (d). (e) was showed the ROS integration as mean values of total photon counts over 1500 second in (d). (**f**) Colony-forming units (cfu) of *Pto* DC3000 bacteria after syringe

bioRxiv preprint doi: https://doi.org/10.1101/2021.10.13.464316; this version posted October 15, 2021. The copyright holder for this preprint (which was not certified by peer review) is the author/funder, who has granted bioRxiv a license to display the preprint in perpetuity. It is made available under aCC-BY-NC-ND 4.0 International license.

874 inoculation for 3 days. (**g**) MAPK activity following 0.1 μM flg22 or 1 μM RALF1
875 treatment for 10 min in WT, *car14569*–Δ10, and *car14569*–Δ20, respectively.

876 All experiments were replicated three times with similar results. Data are shown as the
877 mean ± s.d.; ***$p < 0.001$, n.s., not significant. One–way ANOVA with Tukey's test.

878